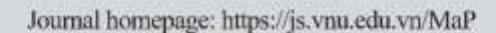


VNU Journal of Science: Mathematics - Physics





Original Article

Tailoring of Thermosensitive Ultrasonic and Mechanical Properties of ϵ -Fe₃N

Roshni Srivastava*, Ramanshu Prabhakar Singh, Giridhar Mishra

Department of Physics, Prof. Rajendra Singh (Rajju Bhaiya), Institute of Physical Sciencesfor Study and Research Veer Bahadur Singh Purvanchal University, Jaunpur-222003, U.P. India

Received 23rd May 2025 Revised 04th June 2025; Accepted 11th June 2025

Abstract: This work examines the mechanical and thermal properties of ε -Fe₃N, a material with a hexagonal crystal structure (hcp). The ε -Fe₃N's hcp structure allows for a broad range of nitrogen stoichiometry, which can be adjusted to enhance its properties. Fe₃N is a promising contender for upcoming energy technologies due to its unique properties, including high catalytic activity and thermal stability. Its structure contributes to efficient heat dissipation and enhanced mechanical behavior at elevated temperatures. Here, the hcp ε -Fe₃N has been characterized by a potential model. First, we computed higher-order elastic constants (HOECs) and then mechanical properties using the HOECs constants at various temperatures. The material's mechanical characteristics give information about its inherent qualities and stability. Additionally, we have determined the specific heat, thermal conductivity, Debye temperature, and ultrasonic velocities at various temperatures. Finally, all relevant parameters are used to determine the ultrasonic attenuation. The results obtained are consistent with the information found in the other works.

Keywords: HOECs, mechanical and thermal properties, attenuation.

1. Introduction

According to studies, ε-Fe₃N exhibits strong magnetic properties, maintaining a high Curie temperature of approximately 522 K for nanoparticles and 575 K for bulk material. This high Curie temperature is beneficial for magnetic devices because it enables the material to maintain its magnetic characteristics at high temperatures. Interpreting the material behavior during the nitriding process, a thermochemical surface treatment technique designed to increase steel's corrosion and wear resistance, requires an understanding of the thermodynamics of Fe–N phases [1].

E-mail address: roshni150690@gmail.com

^{*} Corresponding author.

The substantial temperature dependency of ε-Fe₃N nanoparticles' saturation and remanent magnetization further highlights the material's magnetic stability. It has been demonstrated that selfsustaining reactions at high temperatures, usually between 550 and 850 K, can synthesize ε-Fe₃N [2]. This temperature range is crucial since it affects the final material's stability and phase composition. Furthermore, the structural integrity and magnetic characteristics of the produced ε-Fe₃N can be impacted by the presence of carbon during the nitridation process [3]. Processing methods can alter Fe₃N's mechanical characteristics. For instance, techniques like friction stir processing have been demonstrated to improve the mechanical qualities and modify the microstructure of comparable materials. Because smaller grains have greater grain boundary area to prevent dislocation motion, refining grain size can result in a notable gain in strength and ductility [4]. There are various synthesis techniques to characterize hcp material. Hydrogel-bridged nitridation procedures are a well-known avenue for the synthesis of hcp Fe₃N. With this method, a hydrogel is created by combining precursors such as chitosan and iron salts, and it is then put through a nitridation process. This process has been demonstrated to produce Fe₃N nanoparticles encased in a carbon matrix, improving their electrocatalytic capabilities for reactions like oxygen reduction [5]. Its microstructure and nitrogen content greatly influence the hardness of ε-Fe₃N. According to studies, Nitriding treatments can increase the surface hardness of steel substrates by forming ε-Fe₃N. Incorporating ε-Fe₃N during plasma nitriding operations can enhance surface hardness values to 1140 HV, indicating a significant improvement in mechanical strength [6]. The mechanical properties of hcp Fe₃N, including its hardness and wear resistance, are crucial for its use in tool steels and other technical materials. The nitriding process, which inserts nitrogen into the iron matrix, improves these qualities dramatically. Creating the hard nitride phase improves the microhardness of nitrided layers, including ε-Fe₃N [7].

Hcp ϵ -Fe₃N has been characterized using various methods. To our knowledge, no one has used the potential approach to investigate the ultrasonic properties of ϵ -Fe₃N.

One of the greatest methods for investigating the properties of the material is the ultrasonic non-destructive evaluation technique. There aren't many studies in the literature on the ultrasonic analysis of ϵ -Fe₃N. The ultrasonic characterization of ϵ -Fe₃N is the main emphasis of this work. The L-J potential model approach was used to first determine the HOECs of the selected material at various temperatures to assess ultrasonic properties. These values were then used to assess ultrasonic velocities, thermophysical properties, and total attenuation of the chosen material.

2. Theory

2.1. Theory of Elastic Constants

HOECs can be found using a variety of techniques. The potential model technique is the simplest because it only requires the fundamental lattice parameters and has the fewest restrictions. The L-J potential can be used to formulate HOECs for hcp-structured materials. The higher-order elastic constants (C_{II} and C_{IIK}) of chosen materials can be computed using the provided formulas [8].

```
C_{12}=5.918p^4C'
C_{11}=24.1p^4C^4
                                                                                                                  (1)
C_{13} = 1.925 p^6 C'
                                                              C_{33}=3.464p^8C^4
C_{44} = 2.309 p^4 C'
                                                              C_{66} = 9.851 p^4 C'
                                                              C_{112} = 19.168p^2 B - 1.61p^4 C'
C_{111}=126.9p^2B+8.853p^4C'
C_{113}=1.924p^4B+1.155p^4C'
                                                               C_{123} = 1.617p^4 B - 1.155p^6 C'
C_{133} = 3.695 p^6 B
                                                               C_{155}=1.539p^4B
C_{144} = 2.309 p^4 B
                                                                C_{344} = 3.464 p^6 B
C_{222} = 101.039 p^2 B + 9.007 p^2 C'
                                                               C_{333}=5.196p^8B
```

Here, p = c/a $C' = x \frac{a}{p^5}$, $B = \Psi \frac{a^3}{p^3}$, $x = \frac{1}{8} \left[\frac{nb_{0(n-m)}}{(a^{n+4})} \right]$, and $\psi = -\frac{x}{6a^2(m+n+6)}$ Where m, n denote integers and b_0 denotes L-J parameter [9].

The physical quantities of the material, Y, B, G, and σ , have been computed by the provided formulas [10].

$$Y = \frac{9GB}{G+3B}, B = \frac{B_V + B_R}{2}, G = \frac{G_V + G_R}{2}, B_V = \frac{2(C_{11} + C_{12}) + 4C_{13} + C_{33}}{9}, B_R = C^2/M, G_V = \frac{M+12(C_{44} + C_{66})}{30}, G_R = \frac{5C^2C_{44}C_{66}}{2[3B_VC_{44}C_{66} + C^2(C_{44}C_{66})]'}$$

$$M = C_{11} + C_{12} + 2C_{33} - 4C_{13}$$

$$C^2 = (C_{11} + C_{12})C_{33} - 4C_{13} + C_{13}^2, \sigma = \frac{3B-2G}{2(3B+G)}$$

2.2. Theory of Ultrasonic Velocity

Ultrasonic velocity, which is linked to HOECs, can be used to explain the material's anisotropic behavior. In the acoustic realm, velocities can be classified as V_L , V_{S1} and V_{S2} depending on the mode of atomic vibration. These velocities depend on which direction the wave travels from the hexagonal crystal's special axis. Hexagonal materials' ultrasonic velocities as a function of the angle formed by the unique axis and the direction of propagation are [11].

$$V_{L}^{2} = \frac{\left[C_{33}cos^{2}\theta + C_{11}sin^{2}\theta + C_{44} + \left\{ \left(C_{11}sin^{2}\theta - C_{33}cos^{2}\theta + C_{44}(cos^{2}\theta - sin^{2}\theta)\right)^{2} + 4cos^{2}\theta sin^{2}\theta (C_{13} + C_{44})^{2} \right\}^{1/2}\right]}{2\rho}$$
(3)

$$V_{S1}^{2} = \frac{\left[C_{33}cos^{2}\theta + C_{11}sin^{2}\theta + C_{44} - \left\{\left(C_{11}sin^{2}\theta - C_{33}cos^{2}\theta + C_{44}(cos^{2}\theta - sin^{2}\theta)\right)^{2} + 4cos^{2}\theta sin^{2}\theta\left(C_{13} + C_{44}\right)^{2}\right\}^{1/2}\right]}{2\rho}$$
(4)

$$V_{S2}^{2} = \frac{[C_{44}cos^{2}\theta + C_{166}sin^{2}\theta]}{\rho}$$
 (5)

Here V_L = Longitudinal velocity;

 V_{S1} = Quasi-shear velocity;

 V_{S2} = Shear velocity;

 ρ = density of material;

 θ = angle of unique axis.

The density of a material with an hcp structure can be determined using the formula below [11].

$$\rho = \frac{2Mn}{3\sqrt{3}a^2cN_4} \tag{6}$$

Where M molecular mass, n, number of atoms per unit cell, N_A Avogadro number, a, and c are lattice parameters.

Debye average velocity (V_D) along the unique axis, for wave propagation at any angle is defined as [12]

$$V_D = \left[\frac{1}{3} \left(\frac{1}{V_L^3} + \frac{1}{V_{S1}^3} + \frac{1}{V_{S2}^3} \right) \right]^{-1/3} \tag{7}$$

By using the Debye average velocity V_D , We can compute the Debye temperature θ_D , which is indirectly connected to the HOECs [13, 14].

$$\theta_D = \frac{h}{K_R} \left(\frac{3nN_A \rho}{4\pi M} \right)^{1/3} \tag{8}$$

where h Planck's constant, K_B Boltzmann constant and M molecular mass.

We used the Debye model of heat capacity to calculate the Thermal energy density (E_0) and heat capacity (C_V) .

Electron-phonon, phonon-phonon, and thermo-elastic interactions are main reasons for attenuation in nonmagnetic crystalline materials. Because the mean free pathways of electrons and phonons are incomparable, the attenuation caused by electron-phonon interactions becomes less obvious at higher temperatures. Consequently, at high temperatures, the phonon-phonon and thermo-elastic processes are increasingly important in producing observable attenuation of ultrasonic waves. The attenuation coefficient associated with the loss mechanism, which is caused by phonon-phonon interactions, is represented by the given expression [15].

$$\alpha_{AKh} = \frac{\omega^2 \tau \Delta C}{2\rho V^3 (1 + \omega^2 \tau^2)} \tag{9}$$

In this context, ω represents the angular frequency, V denotes velocity, ΔC refers difference in the moduli, and τ for thermal relaxation time.

As an ultrasonic wave travels through the crystalline material, heat oscillates and transfers heat from the ultrasonic energy. The following formula can be used to quantify thermo-elastic loss.

$$\alpha_{th} = \frac{\omega^2 \langle \gamma_j^i \rangle^2 kT}{2\rho V_L^5} \tag{10}$$

Therefore, the entire ultrasonic attenuation can be obtained by adding, α_{AKh} and α_{th} .

3. Results and Discussion

Lattice characteristics found in the literature are used to compute the SOECs and elastic moduli B, G, and Y of the selected material throughout a temperature range of 300 K to 618 K. Figure 1 illustrates how SOECs change as the temperature rises.

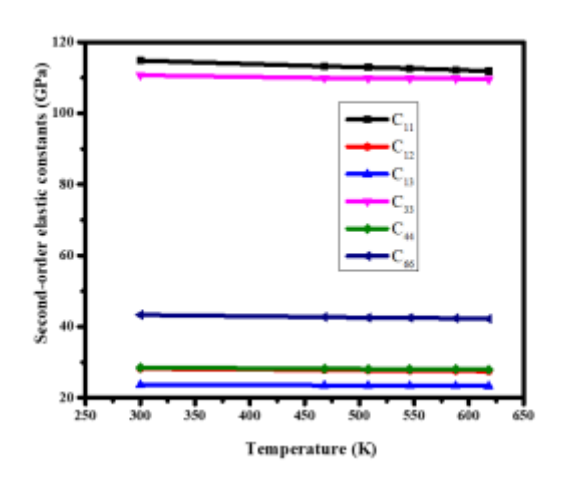


Figure 1. Temperature-dependent second-order elastic constants.

It is observed that SOECs also satisfy the stability criteria, i.e. $(C_{44} > 0, C_{11} > |C_{12}|, (C_{11} + 2C_{12})C_{33} > 2C_{13}^2)$ [16], which means the chosen material is mechanically stable. Higher-order elastic constant values are unavailable for comparison with our findings. However, the produced graph matches that of the literature [17]. We may conclude that our solution provides good agreement.

Figure 2 shows the variation of mechanical properties with an increase in temperature. Here we can observe that as the temperature increases, mechanical properties such as Bulk modulus (B), Shear modulus (G), and Young's modulus (Y) decrease, which is the same as discussed in reference [16].

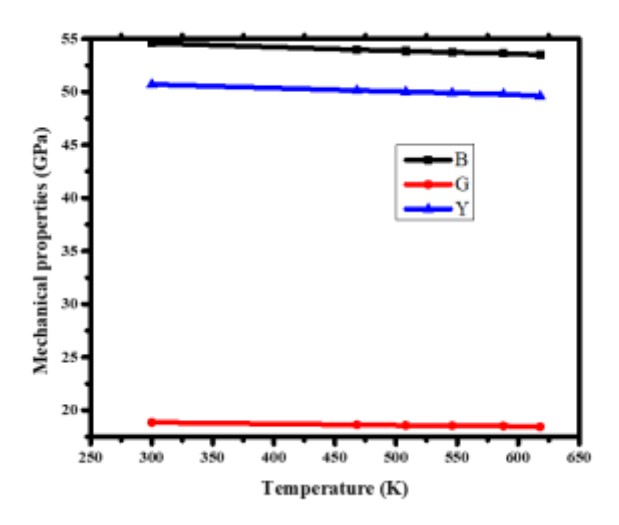


Figure 2. Temperature-dependent Mechanical properties (B, G, Y).

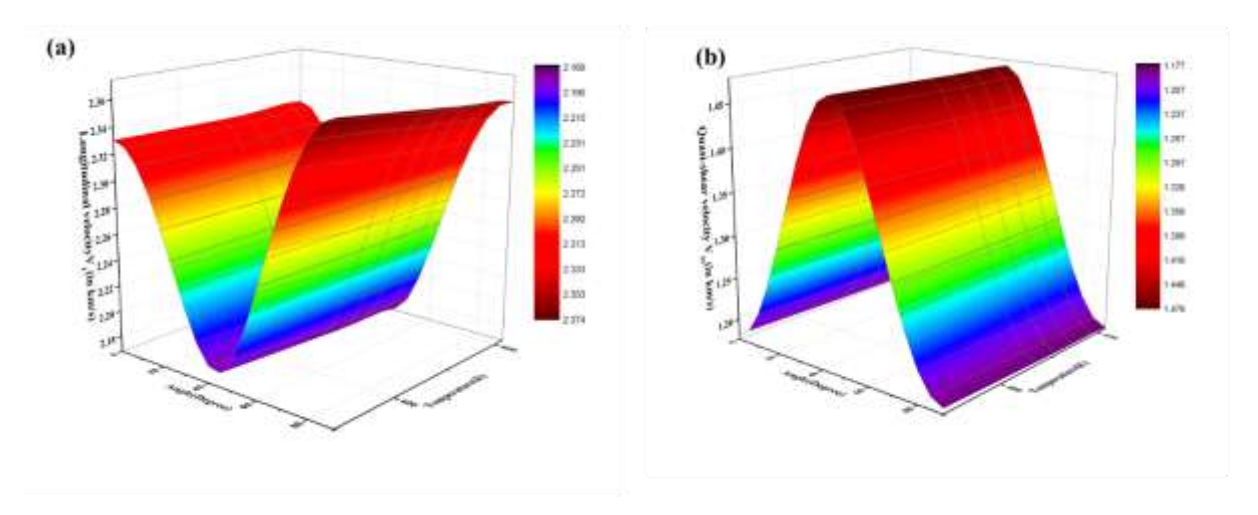


Figure 3. Temperature-dependent (a) longitudinal velocity (V_L) ; (b) Quasi-shear velocity (V_{S1}) .

It is often acknowledged that materials' acoustic characteristics are extremely important. The study of ultrasonic attenuation requires knowledge of HOECs as well as how they change with temperature.

Between the temperatures of 300 to 618 K, ultrasonic velocities (V_L , V_{S1} and V_{S2}) at various angles along the unique axis are computed using the density of hcp-structured material and second-order elastic

constants. Fig. 3 displays the temperature-dependent changes in longitudinal velocity V_L and quasi-shear velocity V_{S1} .

Longitudinal velocity (V_L) rises from 0 to 45° with the unique axis and falls from 45° to 90°, even while quasi-shear velocity (V_{S1}) Increases from 0 to 45° and falls from 45° to 90°. According to the computation, the maximum longitudinal velocity is 2.37367 km/s, and the quasi-shear velocity is 1.47742 km/s at 300 K.

Temperature-dependent variation in ultrasonic shear velocity (V_{S2}) and average Debye velocity (V_D) are presented in Fig. 4.

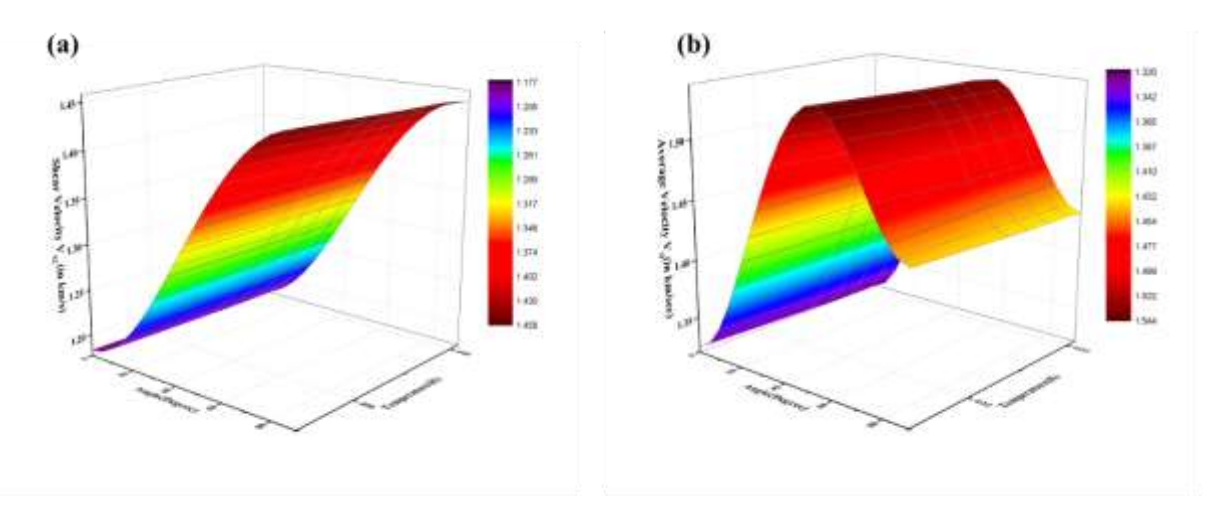


Figure 4 Temperature-dependent (a) shear velocity (V_{S2}) ; (b) Average Debye velocity (V_D) .

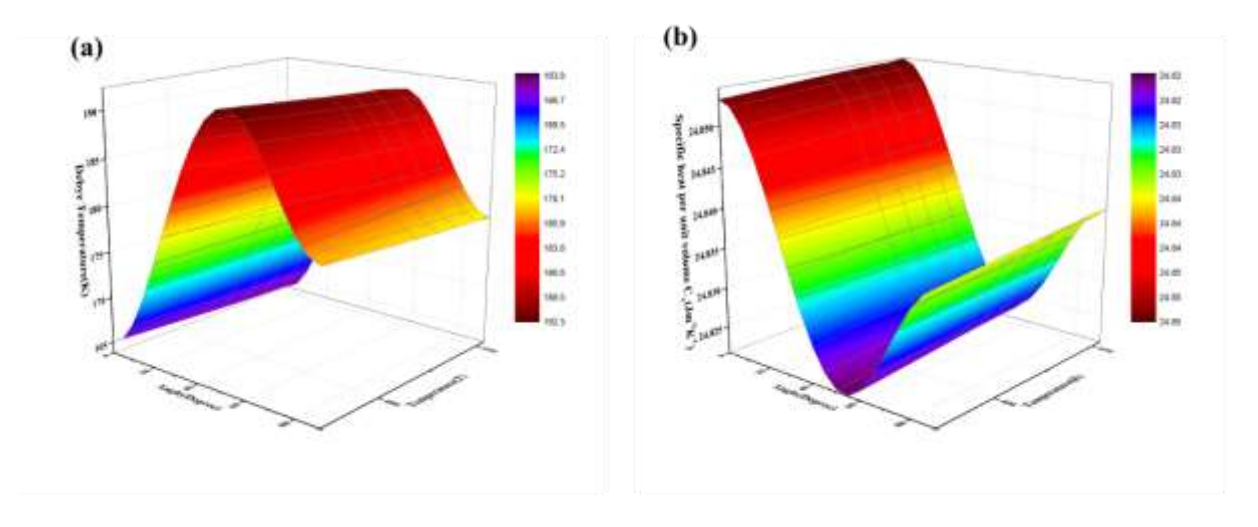


Figure 5. Temperature-dependent (a) Debye temperature (θ_D); (b) Specific heat per unit volume (C_V).

As the θ rises, the V_{S2} rises uniformly and reaches its maximum value of 1.45792 km/s at 300 K for the unique axis 90° angle. Similar to quasi-shear velocity (V_{S1}), Debye's average velocity (V_D) reaches its highest value at 300 K in the temperature range 300 K-618 K at an angle of unique axis $\theta = 55^{\circ}$, which is 1.54318 km/s. Here we discovered that all three velocities. V_L , V_{S1} , and V_{S2} decreases as the temperature rises [18]. All these phenomena are the same as described in literature [19].

It was determined theoretically that higher temperatures cause lattice expansion, which in turn lowers the Debye temperature by inversely affecting vibrational frequencies [20]. As unique axis angle increases θ_D rises. After reaching its maximum, θ_D starts to drop. Debye temperature drops with rising temperature; the highest value of Debye temperature must be determined 192.81 K at 300 K for a 55° angle of the unique axis, within the 300 K–618 K temperature range.

It has been observed in Fig. 6 as angle of unique axis increases, the thermal energy density falls.

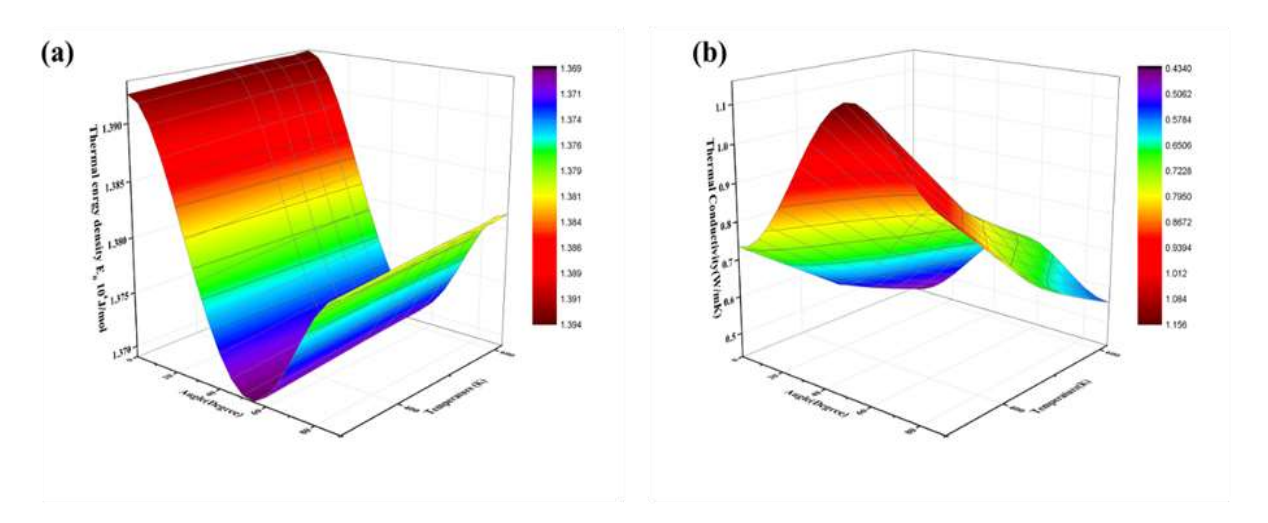


Figure 6. Temperature-dependent (a) thermal energy density E_0 (b) thermal conductivity (T_K) .

For 300 K, the maximum thermal energy must be determined at 13924.28 J/mol at 0⁰. Conversely, when the angle of the unique axis increases, thermal conductivity increases as well. As we know rise in temperature is the reason for the fall in thermal conductivity [21]. In Fig. 6, it is clear that thermal energy density and thermal conductivity both decrease with a temperature rise means our result has the same characteristics as described in reference [18].

The relationship between ultrasonic velocity and temperature in emulsions shows that attenuation and velocity vary considerably around crystallization temperatures. According to these results, temperature-driven structural phase shifts can significantly alter the behavior of ultrasonic waves [22]. Thermoelastic processes and phonon-phonon interactions influence ultrasonic attenuation. The overall ultrasonic attenuation is influenced by variables like ultrasonic velocity, Akhieser damping, etc. This suggests that the HOECs and total attenuation of chosen substance are related to each other indirectly. The Akhieser theory states that the ultrasonic attenuation of longitudinal waves is much greater than thermoelastic attenuation [23].

In this work, we have demonstrated how ultrasonic attenuation coefficients, when measured along a particular axis, vary with temperature and angle. As seen in Fig. 7(a)-(d), this can be illustrated by comparing the ultrasonic attenuation plots.

The plot clearly shows that longitudinal ultrasonic attenuation has the same properties as described in reference 19, with an angle of 45 degrees along the unique axis and a peak value of 8.45×10^{-15} Nps²m⁻¹ at 300 K. Likewise, shear and thermal ultrasonic attenuation exhibit consistent behavior as described in reference [19], with maximum value of 3.06×10^{-16} Nps²m⁻¹ and 2.99×10^{-23} Nps²m⁻¹ for the angle of unique axis 0^0 and 45^0 respectively.

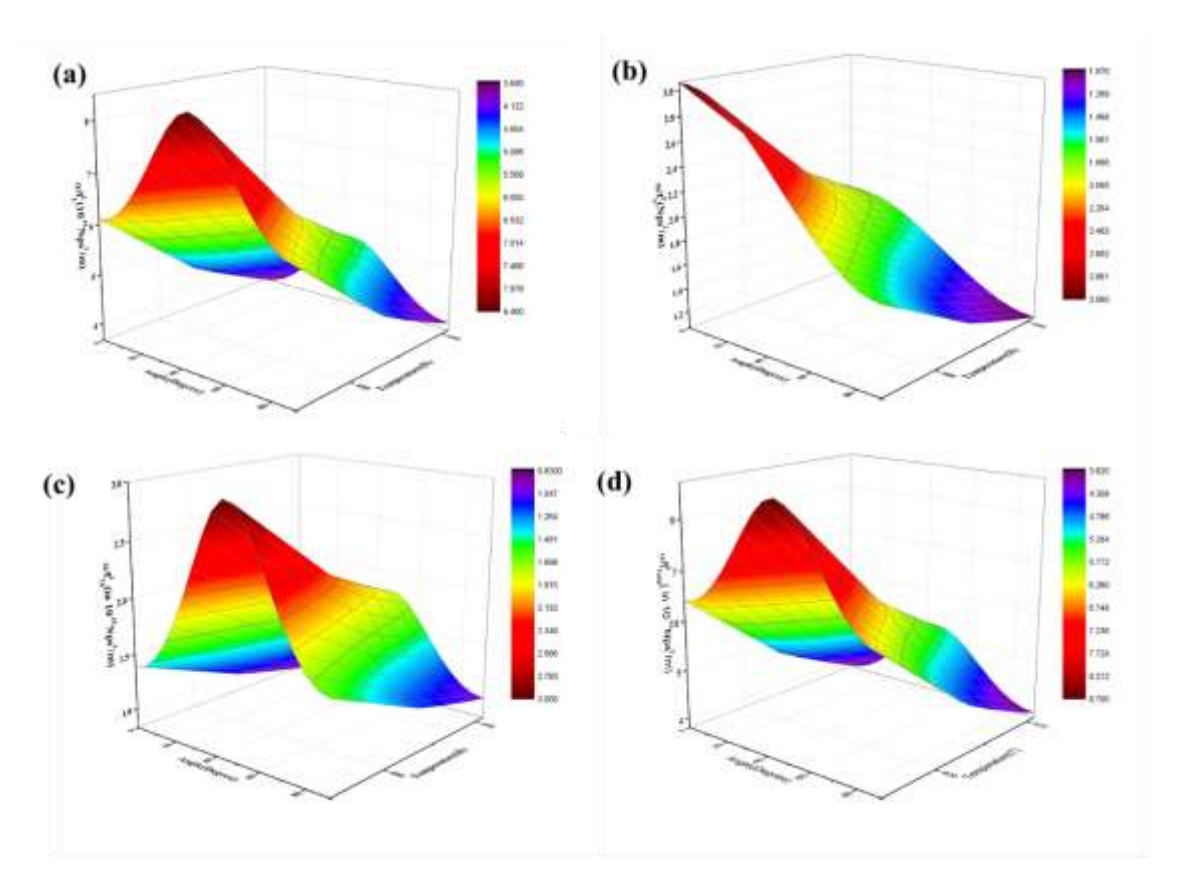


Figure 7. Temperature-dependent (a) longitudinal α/f_L^{2} ; (b) s hear α/f_s^{2} ; (c) thermoelastic α/f_{Th}^{2} ; (d) total α/f_{total}^{2} ultrasonic attenuation.

4. Conclusion

The following conclusion has been reached in light of the previously described findings and discussion.

We were able to assess the elastic constants of hexagonal closed-packed structured ϵ -Fe₃N metal by using the Lennard-Jones potential.

Because of its mechanical and elastic characteristics, the ε-Fe₃N metal shows anisotropic behavior.

Thermoelastic losses are also seen, and the longitudinal mode loss is more important than the shear mode loss.

At an angle of 45°, the total attenuation is found to be maximum at 300 K.q.

Acknowledgement

The authors acknowledge the GSU grant under the PMUSHA scheme of the Government of India.

Data Availability Statement

The authors declare that the data supporting the findings of this study are available within the paper and its supplementary information files.

References

- [1] M. Bakkedal, S. Shang, Z. Liu, Generalization of First-principles Thermodynamic Model: Application to Hexagonal Close-Packed ε-Fe3N, Computational Material Science, Vol. 110, 2016, pp. 83-89, https://doi.org/10.1016/j.commatsci.2016.01.022.
- [2] A. Mukasyan, S. Roslyakov, J. Pauls, Nanoscale Metastable σ-Fe 3 N Ferromagnetic Materials by Self-Sustained Reactions, Inorganic Chemistry, Vol. 58, 2019, pp. 5583-5592, https://doi.org/10.1021/acs.inorgchem.8b03553.
- [3] P. Zhang, X. Wang, W. Wang, Synthesis and Magnetism of ε-Fe3N Submicrorods for Magnetic Resonance Imaging, Dalton Transaction, Vol. 45, 2015, pp. 296-299, https://doi.org/10.1039/c5dt03762j.
- [4] N. Meena, A. Rao, S. Dommeti, N. Prabhu, Effect of Multi-Pass Friction Stir Processing on Microstructure and Mechanical Properties of a Metastable Dual-Phase High Entropy Alloy, Lubricants, Vol. 11, 2023, pp. 1-19, https://doi.org/10.3390/lubricants11010002.
- [5] F. Guo, M. Zhang, S. Yi, Metal-coordinated Porous Polydopamine Nanospheres Derived Fe3N-Feco Encapsulated N-Doped Carbon as a Highly Efficient Electrocatalyst for Oxygen Reduction Reaction, Nano Research Energy, Vol. 1, 2022, pp. 1-8, https://doi.org/10.26599/NRE.2022.9120027.
- [6] I. Öksüzcan, D. Çakan, M. Yilmaz, O. Ertuğrul, Investigation of the Effect of Heat Treatment Conditions on Hardness Properties of Maraging Steels Produced by Additive Manufacturing, Int J 3D Print Technol Digit Ind, Vol. 5, 2021, pp. 654-662, https://doi.org/10.46519/ij3dptdi.1024485.
- [7] A. Yilmaz, H. Aydin, Friction-Wear Characteristics of Plasma Nitrided Cold-Work Tool Steels, Uludağ Univ J Fac Eng, Vol. 25, 2020, pp. 609-622, https://doi.org/10.17482/uumfd.630430.
- [8] B. Jyoti, S. Singh, M. Gupta, Investigation of Zirconium Nanowire by Elastic, Thermal and Ultrasonic Analysis, Zeitschrift fur Naturforsch - Sect A J Phys Sci, Vol. 75, 2020, pp. 1077-1084, https://doi.org/10.1515/zna-2020-0167.
- [9] W. Mason, T. Bateman, Relation between Third-Order Elastic Moduli and the Thermal Attenuation of Ultrasonic Waves in Nonconducting and Metallic Crystal, J Acoust Soc Am, Vol. 40,1966, pp. 852-862.
- [10] A. Maddheshiya, N. Yadav, S. Singh, Mechanical, Elastic and Microstructural Investigations on HCP Phase High-Entropy Alloys, Mapan J Metrol Soc India, Vol. 38, 2023, pp. 1019-1026, https://doi.org/10.1007/s12647-023-00674-6.
- [11] C. Yadav, D. Pandey, D. Singh, Ultrasonic study of Laves phase compounds ScOs2 and YOs2, Indian J Phys, Vol. 93, 2019, pp. 1147-1153, https://doi.org/10.1007/s12648-019-01389-8.
- [12] D. Pandey, S. Pandey, Ultrasonics: A Technique of Material Characterization. In: Dissanayake D (ed) Acoustic Waves. IntechOpen, 2010, pp. 398-430.
- [13] R. Singh, S. Yadav, A. Tiwari, G.Mishra, Theoretical Investigation of Mechanical and Thermal Features in ScTiZr and ScTiHf Alloys: A Comparative Study, J Pure Appl Ultrason, Vol. 45, 2023, pp. 55-59.
- [14] R. Singh, S. Yadav, G. Mishra, D. Singh, Pressure Dependent Ultrasonic Properties of Hcp Hafnium Metal, Zeitschrift für Naturforsch - Sect A J Phys Sci, Vol. 76, 2021, pp. 549-557, https://doi.org/10.1515/zna-2021-0013.
- [15] R. Srivastava, R. Singh, G. Mishra, Study of Mechanical and Thermophysical Properties of Ni 3 Ti, Zeitschrift für Naturforsch A, Vol. 79, 2024, pp. 1135-1142, https://doi.org/10.1515/zna-2024-0093.
- [16] B. Jyoti, S. Singh, M. Gupta, Ultrasonic and Thermophysical Properties of Cobalt Nanowires, Acoust Phys, Vol. 67, 2021, pp. 584-589.
- [17] I. Gülseren, J. Coupland, Excess Ultrasonic Attenuation Due to Solid-solid and Solid-liquid Transitions in Emulsified Octadecane, Cryst Growth Des, Vol. 7, 2007, pp. 912-918, https://doi.org/10.1021/cg060683f.
- [18] R. Singh, S. Yadav, D. Singh, G. Mishra, Theoretical Approach to Investigate Temperature Dependent Ultrasonic and Thermophysical Properties of Ti-Zr-Hf Ternary Alloy, Int J Res Appl Sci Eng Technol, Vol. 10, 2022, pp. 583-588, https://doi.org/10.22214/ijraset.2022.47382.
- [19] A. A. Sheikh, S. Jalal, S. Mawlood, Theoretical High Pressure Study of Phonon Density of State and Debye Temperature of Solid C60: Grüneisen Approximation Approach, Int J Thermodyn, Vol. 25, 2022, pp. 10-15 https://doi.org/10.5541/ijot.900071.
- [20] C. Yu, H. Cheng, W. Chen, Structural, Mechanical, Thermodynamic and Electronic Properties of AgIn2 and Ag3In Intermetallic Compounds: Ab Initio Investigation, RSC Adv, Vol. 5, 2015, pp. 70609-70618, https://doi.org/10.1039/c5ra11142k.
- [21] S. Jiang, Y. Huang, P. Xue, Temperature-dependent Deformation Behavior of a CuZr-based Bulk Metallic Glass Composite, J Alloys Compd, Vol. 858, 2021, pp. 158368, https://doi.org/10.1016/j.jallcom.2020.158368.
- [22] K. M. Raju, Behavior of Ultrasonic Attenuation in MnO, Open J Acoust, Vol. 03, 2013, pp. 54-59, https://doi.org/10.4236/oja.2013.33a009.
- [23] S. Singh, G. Singh, A. Verma, Mechanical, Thermophysical, and Ultrasonic Properties of Thermoelectric HfX2 (X = S, Se) Compounds, Met Mater Int, Vol. 27, 2021, pp. 2541-2549, https://doi.org/10.1007/s12540-020-00633-9.